Proceedings of the 28th IEEE
EMBS Annual International Conference
New York City, USA, Aug 30-Sept 3, 2006

Epicardial rotors in panoramic optical maps of fibrillating swine ventricles

Matthew W. Kay and Jack M. Rogers

Abstract—**It has been proposed that VF waves emanate from stable periodic sources (often called "mother rotors"). Our objective was to determine if stable rotors are consistently present on the epicardial surface of hearts comparable in size to human hearts. Using new optical mapping technology, we imaged VF from nearly the entire ventricular surface of 6 isolated swine hearts. Using newly developed pattern analysis algorithms, we identified and tracked VF wavefronts and phase singularities (PS). We introduce the notion of a compound rotor in which the rotor's central PS can change and describe an algorithm for automatically identifying such patterns. This prevents rotor lifetimes from being inappropriately abbreviated by wavefront fragmentation and collision events near the PS. We found that stable epicardial rotors were not consistently present during VF: only 1 of 17 VF episodes contained a compound rotor that lasted for the entire mapped interval of 4s. However, shorter-lived rotors were common; 12.2±3.3 compound rotors with lifetime >200 ms were visible on the epicardium at any given instant. We conclude that epicardial mother rotors do not drive VF in this experimental model; if mother rotors do exist, they are intramural or septal. This paucity of persistent rotors suggests that individual rotors will eventually terminate by themselves and therefore the continual formation of new rotors is critical for VF maintenance.**

I. Introduction

During VF, the ventricles are swept by complexly interacting activation waves and the muscle does not contract in synchrony. VF is generally self-sustaining unless halted by a shock; however, the mechanisms maintaining VF are poorly understood. A key question is whether the multitude of activation waves that characterize VF emanate from one, or possibly a few, stable periodic sources (1), or whether the wave sources are transitory and widely distributed (2). The first mechanism of VF is often called the mother rotor hypothesis. The second mechanism is often called the multiple wavelet hypothesis. Because the two mechanisms suggest different strategies for controlling VF (targeting the central source vs. global interventions), the distinction is likely to be critical in developing new rational anti-VF therapies.

One step in substantiating the mother rotor hypothesis in large hearts is to determine if at least one stable rotor is consistently present during VF. Previous studies that mapped portions of the swine right ventricle (3,12), left ventricle (3,4,6,12), or septum (5) were unable to document such a rotor, even though relatively long-lived rotors were sometimes observed (6). However, all of these studies mapped only a limited region, typically 20-40 cm^2, admitting the possibility that a mother rotor was present, but located in an unmapped region.

The objective of the present study was to map from the entire epicardial surface of a large heart preparation to determine by direct observation if stable epicardial rotors are consistently present during VF. This was accomplished using a newly developed optical mapping system that merges fluorescence data acquired from 4 high-speed video cameras into a single continuous dataset (7) and newly developed algorithms that identify and track wavefronts and PSs as they move over the epicardium (8). In addition, we introduce the notion of a compound rotor in which the central PS can change and describe an algorithm for automatically identifying such patterns.

II. Methods

We studied a total of 17 VF episodes in 6 hearts excised from healthy mixed breed pigs of either sex (weight 23±4 kg, range 21.0-30.2 kg). Details of anesthesia, heart excision, and Langendorff perfusion have been described previously (9).

A. Panoramic Optical Mapping

We used a newly developed optical mapping system that records electrical activity from nearly the entire ventricular epicardium (Figure 1). The shape of the epicardium is acquired with a rotating geometry camera. One rotation is completed in 70s. Epicardial models are constructed with sub-millimeter resolution and decimated to ~1.6 mm. Electrical activity is recorded using a voltage sensitive dye and the 4 mapping cameras (iXon DV860, Andor Technology, South Windsor, CT). Final spatial resolution is ~1.6 mm and temporal sampling is 750fps. Fluorescence data from the mapping cameras are merged into one dataset by mapping them onto the epicardial geometry. Other details have been previously described (7).

This work was supported by NIH grant HL64184 (JMR) and a grant from the Whitaker Foundation (MWK).

M.W. Kay was with the Dept. of Biomedical Engineering at the University of Alabama in Birmingham. He is now with the Dept. of Pharmacology and Physiology at The George Washington University in DC (phymwk@gwumc.edu).

J.M. Rogers is with the Dept. of Biomedical Engineering at the University of Alabama in Birmingham. (jmr@crml.uab.edu).

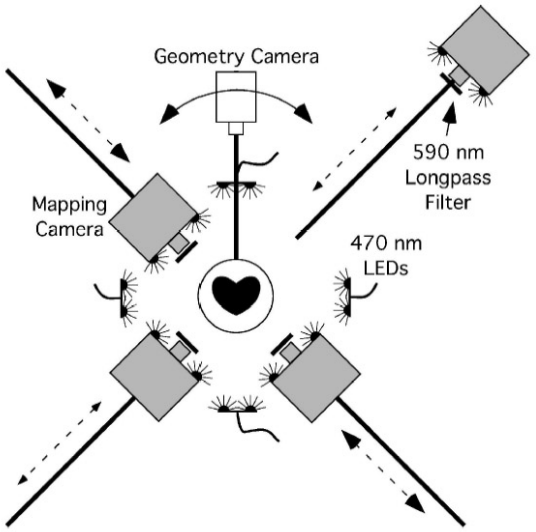

Figure 1: Schematic of the panoramic optical mapping system.

B. Study Protocol

Hearts were immobilized with 2,3-butanedione monoxime (BDM, 20 mM) to eliminate contraction artifacts and stained with the voltage-sensitive dye di-4-ANEPPS (15 μM). After a stabilization period, the following procedure was repeated three times: 1) scan the epicardial geometry; 2) optically map four seconds of a paced rhythm; 3) induce VF by applying a 9V battery to the right ventricle; 4) ~20 seconds after induction, optically map 4 seconds of VF; 5) defibrillate with a minimum reliable-strength shock (5-20 J) delivered through external paddles. At the end of each experiment, all cameras were calibrated as previously described (7).

C. Compound Rotors

In the traditional definition of a rotor, a wavefront propagates about a single PS (10). However, we commonly observed wave fragmentation or collision events near the PS at the tip of a rotating wavefront. In such events, the original PS was annihilated, but a wavefront continued to rotate in the same direction about a new PS in very nearly the same position. Figure 2 shows an example of this phenomenon. In panel A, wavefront 1 is rotating counterclockwise about PS i. By panel B, wavefront 1 has fragmented into wavefronts 2 and 3. Wavefront 3 contains the original PS i in addition to a new PS of opposite chirality (gray triangle). Wavefront 2 contains another new PS, ii, with the same chirality as i. By panel C, wavefront 3 has contracted allowing the oppositely rotating PSs on either end to annihilate each other and terminate the wavefront. One of the annihilated PSs is the original PS i. However, wavefront 2 now propagates about the new PS ii much as wavefront 1 propagated about PS i. It can be argued that such a pattern constitutes reentry about a single organizing center even though the central PS changes.

We developed an algorithm to automatically detect these events. We create, for each VF episode, two new directed graphs (11) called singularity graphs. There is one such graph for each of the two chiralities. To generate a singularity graph, we first set the chirality-appropriate PSs to be the singularity graph's nodes. We then iterate over all contact events in the VF episode's wavefront graph. The wavefront graph for the activation pattern in Figure 2 A-C is shown in panel D. This graph contains one contact event, the fragmentation of wavefront 1 into wavefronts 2 and 3. For each contact, we identify the PSs that continue through the contact (e.g., PS i) and those that either begin or end at the contact. PS ii is an example of a beginning PS. We compute the spatial distance between each continuing PS and each beginning or ending PS. If this distance is no more than 5 triangle-to-triangle hops (~8 mm), a graph edge is added between the two corresponding PSs. The edges are directed from continuing-to-beginning or ending-to-continuing PSs. The singularity graph for the black singularities in Figure 2 A-C is shown in panel E. There are two nodes (i and ii) and a single edge directed from i to ii. Although we have described the algorithm with a fragmentation event, it works in the same way for collisions.

A singularity graph may contain multiple subgraphs each of which is disconnected from all other subgraphs. In graph theory, each of these subgraphs is called a component of the full graph (11). In the limiting case of a VF episode in which no events such as the one depicted in Figure 2 A-C occurred, both singularity graphs (one for each chirality) would consist only of nodes with no connecting edges. Each node would therefore be its own component. The singularity graph in Figure 2 E is the opposite limiting case: all nodes are connected by edges and the entire graph therefore consists of a single component spanning all PSs. We treat each singularity graph component as a compound rotor. **A compound rotor contains one or more PSs, all of which have the same chirality.** The number of PSs in the compound rotor is the number of nodes in the singularity graph component. Its lifetime spans the lifetimes of all of its constituent PSs.

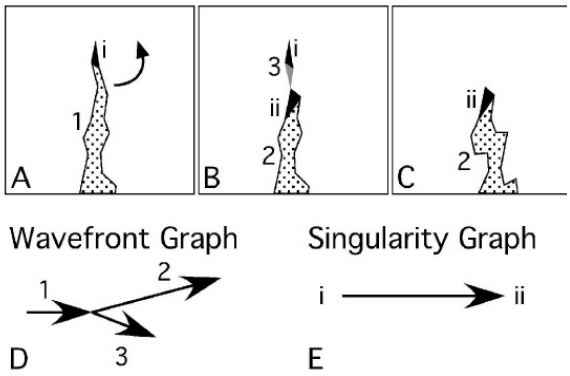

Figure 2: A compound rotor with two sequential PSs. Panels A-C: the black and gray triangles are PSs of opposite chirality and the stippled regions are wavefronts. The arrow in A indicates the direction of rotation about the PS. Panel D: a wavefront graph of the activation pattern in A-C. Panel E: the singularity graph of the

III. RESULTS

Each VF episode was mapped for 4s starting ~20s after induction. Figure 3 shows a snapshot of a panoramically mapped VF episode. Over all VF episodes, we observed 310,356 PSs. Most PSs were very short in duration: 65% had lifetimes less than 10 ms and 99.6% were less than 200 ms. PSs lasting longer then 200 ms have completed at least one cycle of reentry, but less than two. Figure 4 shows a histogram of all PS lifetimes. Only one PS persisted for its entire mapped interval.

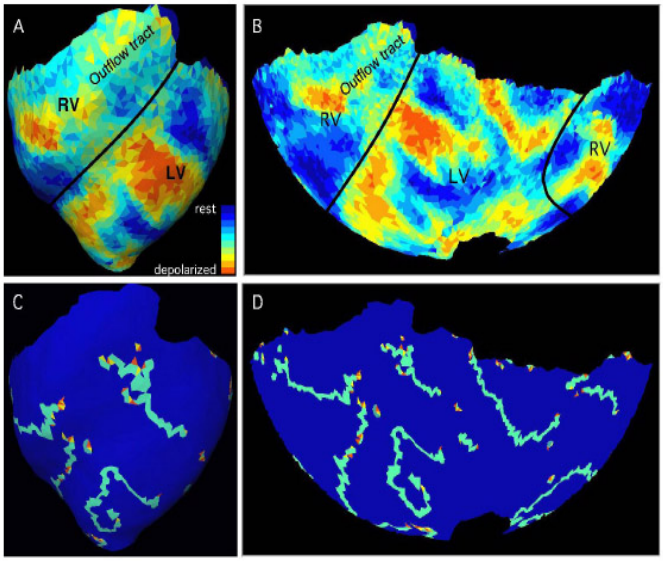

Figure 3: One frame of a VF episode. Panels A and B show fluorescence data. The black lines indicate the approximate boundary between the right and left ventricles. Panels C and D show the wavefronts (light blue triangles) and phase singularities found in the same frame. Yellow and orange phase singularities have opposite chiralities. Panels A and C show an anterior view of the reconstructed epicardial geometry. In panels B and D, a Hammer map projection is used to show the entire epicardium.

Combining PSs into compound rotors substantially prolonged lifetimes. Over all VF episodes, there were 1.6±2.0 (mean±std) PSs per compound rotor. 79% of compound rotors had only one PS and an additional 10% had only two. The compound rotor with the most PSs had 80.

Figure 4 shows the distribution of compound rotor lifetimes exceeding 200 ms averaged across episodes. Compound rotors lasting longer than 1 s were rare. The lifetime of the longest-lived compound rotor from each episode is listed in Table 1. One episode contained two compound rotors that persisted for the entire mapped interval. None of the other episodes contained a compound rotor that persisted for the entire mapped interval.

Table 1 lists the mean number of compound rotors exceeding 200 ms that were present at one time in each episode. The mean over all episodes was 12.2±3.3. Figure 5 is an example of how the number of compound rotors fluctuates with time. We fit a straight line to these data for each episode (e.g., the dotted line in Figure 5). The mean slope of the regression line over all episodes was -0.3±1.0s^{-1}. This number was not significantly different from 0 by t-test ($p>0.2$); thus the number compound rotors did not consistently increase or decrease during the mapped interval.

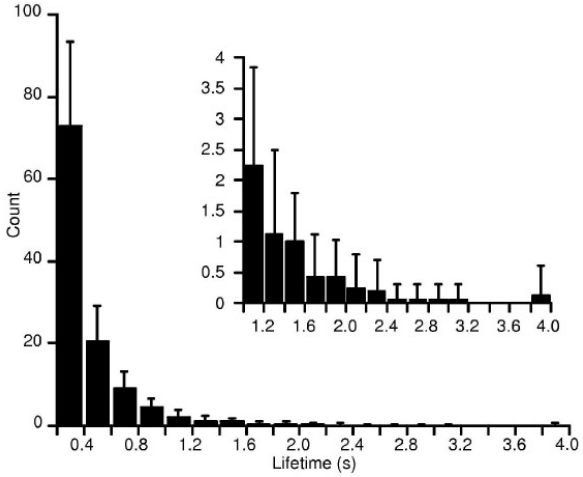

Figure 4: Lifetime distribution for compound rotors that lasted longer than 200 ms. The bars are averages across episodes. Error bars are standard deviations. The inset is an expansion showing lifetimes exceeding 1.0 s.

Table 1. *Compound Rotor Parameters per Episode*

Animal	Episode	maxLifetime* (s)	nRotors†
1	1	1.001	8.8 ± 2.2
1	2	1.289	11.9 ± 2.4
1	3	1.120	9.2 ± 2.8
2	4	1.480	9.1 ± 3.4
2	5	1.404	9.4 ± 3.0
2	6	1.916	12.9 ± 3.4
3	7	1.876	15.7 ± 3.8
3	8	2.665	13.9 ± 3.0
4	9	3.081	11.3 ± 2.7
4	10	1.953	9.7 ± 2.5
4	11	3.981	8.1 ± 2.3
5	12	1.761	12.1 ± 3.1
5	13	2.047	20.3 ± 4.8
5	14	2.425	10.4 ± 2.7
6	15	1.877	14.4 ± 3.0
6	16	1.457	13.9 ± 3.5
6	17	2.292	16.7 ± 3.8

* Maximum compound rotor lifetime

† Mean number of compound rotors present at any instant (± std)

IV. DISCUSSION

Our major finding is that stable epicardial rotors are not consistently present during VF in this experimental model.

All 17 VF episodes contained compound rotors that lasted for hundreds of milliseconds and each had at least one compound rotor that lasted for 1 s or more. However, a compound rotor cannot drive the VF episode (i.e., be a mother rotor) unless it persists for the entire episode. Only one of the 17 VF episodes we analyzed contained compound rotors that lasted for the entire mapped interval. Previous epicardial mapping studies were unable to document mother rotors in either the left (3,4,6) or right (3) ventricle. However, these studies could not exclude epicardial mother rotors because only limited epicardial regions were sampled.

In the present study, we used a newly developed optical mapping system (7) that can identify and track VF wavefronts across nearly the entire epicardium. Thus we extend the previous results and exclude stable epicardial rotors (with the possible exception of a rotor at the very tip of the apex) as a requirement for VF maintenance in this experimental model.

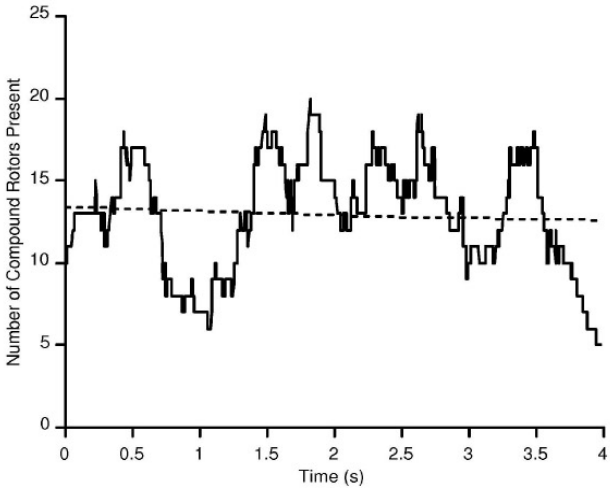

Figure 5. Temporal fluctuation in the number of compound rotors (with lifetimes exceeding 200 ms) simultaneously present on the epicardium. Data are from episode 6 in Table 1. The dotted line is a linear regression line.

The possibility still exists that VF in pig hearts is driven by a stable mother rotor whose filament does not intersect the epicardium and therefore cannot be observed directly with epicardial mapping. However, stable mother rotors were not observed in studies mapping limited nonepicardial regions including the septum (5) and sections across the right (12) and left (6,12) ventricular free walls. Further studies are needed to confirm or exclude the presence of stable nonepicardial mother rotors.

Despite the paucity of compound rotors that persisted for the entire mapped interval, shorter-lived rotors were common. We found that at any given instant, roughly a dozen (with lifetimes of at least 200 ms) were simultaneously present on the epicardium.

These data suggest that the formation of new rotors is critical for VF maintenance because once started, rotors will eventually die out by themselves. This implies that rotor formation may be a more attractive target than rotor termination in the development of new anti-VF therapies.

V. Limitations

We imaged VF activation patterns with high spatial (~1.6 mm) and temporal (750 frames per second) resolution over the great majority of the swine epicardial surface. However, patterns within the ventricular walls were not recorded. The study focused on VF relatively early after induction (Wiggers' Stage II). Activation patterns are known to change as VF proceeds (13), so our findings may not apply to more prolonged VF. We mapped isolated perfused swine hearts that were exposed to BMD to eliminate motion artifacts in the optical recordings. Other species were not studied. We previously found that VF patterns in this preparation are slower and more regular than those in the same hearts before excision (9). Other authors have found that BDM converts VF to a stable tachycardia in isolated ventricular tissue from dogs (14). In addition, Evans et al. used BDM to stabilize reentry to create a model of monomorphic VT in rabbit hearts (15). Thus, because of the slowing and stabilization effects of heart isolation and BDM on VF, we expect that rotor lifetimes are substantially shorter in intact hearts than they were in the present study.

References

[1] Zaitsev AV, Berenfeld O, Mironov SF, Jalife J, and Pertsov AM. Distribution of excitation frequencies on the epicardial and endocardial surfaces of fibrillating ventricular wall of the sheep heart. Circ Res 86: 408-417, 2000.

[2] Choi BR, Nho W, Liu T, and Salama G. Life span of ventricular fibrillation frequencies. Circ Res 91: 339-345, 2002.

[3] Rogers JM, Huang J, Pedoto RW, Walker RG, Smith WM, and Ideker RE. Fibrillation is more complex in the left ventricle than the right ventricle. J Cardiovasc Electrophysiol 11: 1364-1371, 2000.

[4] Nanthakumar K, Huang J, Rogers JM, Johnson PL, Newton JC, Walcott GP, Justice RK, Rollins DL, Smith WM, and Ideker RE. Regional differences in ventricular fibrillation in the open-chest porcine left ventricle. Circ Res 91: 733-740, 2002.

[5] Huang J, Walcott GP, Killingsworth CR, Melnick SB, Rogers JM, and Ideker RE. Quantification of activation patterns during ventricular fibrillation in open-chest porcine left ventricle and septum. Heart Rhy 2: 720-728, 2005.

[6] Rogers JM, Huang J, Melnick SB, and Ideker RE. Sustained reentry in the left ventricle of fibrillating pig hearts. Circ Res 92: 539-545, 2003.

[7] Kay MW, Amison PM, and Rogers JM. Three-dimensional surface reconstruction and panoramic optical mapping of large hearts. IEEE Trans Biomed Eng 51: 1219-1229, 2004.

[8] Rogers JM. Combined phase singularity and wavefront analysis for optical maps of ventricular fibrillation. IEEE Trans Biomed Eng 51: 56-65, 2004.

[9] Qin H, Kay MW, Chattipakorn N, Redden DT, Ideker RE, and Rogers JM. Effects of heart isolation, voltage-sensitive dye, and electromechanical uncoupling agents on ventricular fibrillation. Am J Physiol, Heart Circ Physiol 284: H1818-H1826, 2003.

[10] Gray RA, Pertsov AM, and Jalife J. Spatial and temporal organization during cardiac fibrillation. Nature 392: 75-78, 1998.

[11] Chachra V, Ghare PM, and Moore JM. Applications of Graph Theory Algorithms. New York: North Holland, 1979.

[12] Valderrabano M, Lee MH, Ohara T, Lai AC, Fishbein MC, Lin SF, Karagueuzian HS, and Chen PS. Dynamics of intramural and transmural reentry during ventricular fibrillation in isolated swine ventricles. Circ Res 88: 839-848., 2001.

[13] Huang J, Rogers JM, Killingsworth CR, Singh KP, Smith WM, and Ideker RE. Evolution of activation patterns during long-duration ventricular fibrillation in dogs. Am J Physiol Heart Circ Physiol 286: H1193-1200, 2004.

[14] Riccio ML, Koller ML, and Gilmour RF. Electrical restitution and spatiotemporal organization during ventricular fibrillation. Circ Res 84: 955-963, 1999.

[15] Evans F, Gray R, and Ideker R. Global effects of shocks on epicardial transmembrane potential. PACE 23: 609, 2000.